A Closed-Form Expression for the Frequency-Dependent Microwave Responsivity of Transistors Based on the I -V Curve and S-Parameters

Gaudencio Paz-Martínez, Philippe Artillan, Javier Mateos, Edouard Rochefeuille, Tomás González, Ignacio Íñiguez-De-La-Torre

A Closed-Form Expression for the Frequency Dependent Microwave Responsivity of Transistors Based on the I-V Curve and S-Parameters

Gaudencio Paz-Martínez, Philippe Artillan, Javier Mateos, *Member, IEEE,* Edouard Rochefeuille, Tomás González, *Senior Member, IEEE,* and Ignacio Íñiguez-de-la-Torre

***Abstract*—A generic high frequency model of two-port RF detectors, based on I-V curves and S-parameters measurements, is proposed and applied to the case of AlGaN/GaN field effect transistors. The expression of the current responsivity (A/W) of any kind of transistor detector is derived for RF power injection both through the gate and the drain. The main novelty of the proposed model is the adequate consideration of the often neglected gate-drain coupling. The developed formalism also clarifies the voltage-current DC bias and the progressive and regressive power waves used to describe the RF excitation of the two-port non-linear device. The obtained frequency dependent closed-form expressions replicate very satisfactorily the current responsivity measurements made in AlGaN/GaN HEMTs up to 67 GHz. In order to improve the physical understanding of the frequency dependence of the current responsivity of transistors, it is expressed in terms of the magnitude and phase of drain-gate voltage ratio. The analysis of the different contributions to the RF responsivity reveals that the gate-drain capacitive coupling plays a key role in its frequency dependence.**

***Index Terms*—GaN high electron mobility transistors (HEMTs), Radio frequency detection, Responsivity model, Zero-bias detector**

I. Introduction

In recent years, the use of Field Effect Transistors (FET) as direct power detectors in the mm and sub-mm wave range is gaining interest [1]. Different technologies have been tested and demonstrated with promising performances: InGaAs/AlInAs HEMTs [2], GaAs HEMTs [3], Si MOSFETs or CMOS structures [4], GaN HEMTs [5], [6], Si FinFETs [7], graphene FETs [8], [9] or nanowire FETs [10]. Initially, the plasma-wave Dyakonov-Shur theory [11] was used to explain the microwave detection with FETs at frequencies above their classical cutoff, leading to the imprecise collective label of "plasma-wave detectors". However, at moderately high frequencies, typically below 100 GHz, the classic quasistatic resistive mixing concept linked to the non-linearity of the I-V curves of the devices [12] is able to perfectly describe the RF detection. At higher frequencies, above the cutoff of amplification, this approximation breaks down and has to be replaced by a non-quasi-static theory, like the non-resonant Dyakonov-Shur plasma detection theory [13]. However, whereas the latter predicts an enhanced responsivity, experimental data show a frequency roll-off, which can be modeled with a fitting parasitic capacitance [14]. Thereby, with strong practical interest for electronics applications such as 5G or 6G wireless communications [15], [1], we will focus on sub-THz frequencies and we will consider that eventual plasma-wave [14] or thermoemission [16] effects can be neglected. The main novelty in our paper is the computation of the frequency-dependent detection response of FETs both taking into account the non-linearity and the frequency dependent behavior thanks to the measured I-V curves and S-parameters. Another key novelty in our approach is to compute the response of the transistor in both cases of gate and drain RF power injection from the measured S-parameters, with no additional steps involving the extraction of a lumped-element equivalent circuit or the use of further approximations (as in ref. [12]). In the two cases, the frequency-dependent contribution of the gate-drain coupling is accurately taken into account. The paper combines the information of the current-voltage DC curves and the progressive/regressive waves related to the S-parameters into the closed-form expressions for the responsivities. We emphasize the importance of properly computing the observable RF voltages $V_{gs}(t)$ and $V_{ds}(t)$ at each terminal of the transistor, as illustrated in Fig. 1, from the available input power (i.e. the progressive waves injected into gate or drain port, V_{gs}^{+} or V_{ds}^{+}, respectively). We provide the closed-form expressions in real units (A/W) for the responsivity of the transistors. The predicted current responsivities with both gate and drain injection schemes are validated with measurements up to 67 GHz in a 0.25 μm gate AlGaN/GaN transistor. To the authors' knowledge, very few papers provide a direct quantitative comparison between measurements and models in a broadband frequency range [12].

II. Experimental Setup

The experimental setup is sketched in Fig. 1, where a two-channel SMU Keysight B2902A and Keysight N5247A PNA-X are used for the measurements. First, the DC I-V curves are measured. Then, the S-parameters at each bias points are obtained. Port 1 corresponds to the gate and port 2 to the

Manuscript received 24 March 2023; accepted 17 June 2023. This work has been partially supported through Grant PID2020-115842RB-I00 funded by MCIN/AEI/10.13039/501100011033. *(Corresponding author: Gaudencio Paz-Martínez)*

G. Paz-Martínez, J. Mateos, T. González and I. Íñiguez-de-la-Torre are with the Applied Physics Department, and USAL-NANOLAB, Universidad de Salamanca, 37008 Salamanca, Spain (e-mail: gaupaz@usal.es, javierm@usal.es, tomasg@usal.es, indy@usal.es).

P. Artillan and E. Rochefeuille are with Univ. Grenoble Alpes, Univ. Savoie Mont Blanc, CNRS, Grenoble INP, IMEP-LAHC, 38000 Grenoble, France (e-mail: philippe.artillan@univ-smb.fr, edouard.rochefeuille@univ-smb.fr).

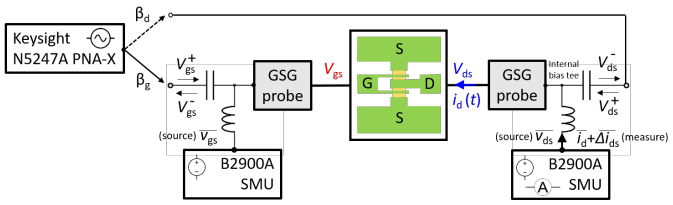

Fig. 1. Schematic drawing of the setup for DC and RF characterization. In this setup, the PNA-X VNA operates as the RF source. The RF power can be injected either in the drain or in the gate port. The two-channel SMU biases in voltage the drain and gate terminals of the transistor. An internal bias-tee allows us to couple DC and RF signals. The drain current is measured as detection output. Ground-signal-ground (GSG) probe tips are used to contact the coplanar waveguide accesses.

drain, and the calibration planes are brought to the transistors terminals thanks to a Short-Open-Load-Thru calibration. Finally, the VNA is employed as RF generator. A low-power signal of -20 dBm from 100 MHz to 67 GHz is injected into the transistor in two configurations: at the drain terminal or at the gate terminal. The losses due to the cables, connectors and probe tips have been adequately compensated [4]. The SMU averages the output DC rectified current at the drain port, thus providing the current responsivities in gate or drain injection conditions (β_d and β_g, defined as $\overline{\Delta i_d}/P_{RF}$, being Δi_d the drain current shift measured when a RF signal of P_{RF} power is injected into the drain or gate ports, respectively, in A/W). Everything is controlled with a home-made LabView code.

III. RF MODEL OF THE RESPONSIVITY

A. Limitations of the Quasi-Static Model

A AlGaN/GaN HEMT similar to that studied in refs. [17], [18], [19], with a gate length L_g=250 nm and a gate width W=2×50 μm, has been used in the experiments. The inset in Fig. 2(a) presents the transistor output curves measured in DC (note that self-heating is negligible for the low voltage conditions used in our experiments). Fig. 2(a) shows, in empty blue symbols, the dependence of β_d on V_{GS} obtained when an RF signal of different frequencies from 1 to 67 GHz is injected at the drain port with V_{DS}=0. These are the standard "zero bias" detection conditions, which allow to minimize the output noise and improve the sensitivity of the detectors. Indeed, the other key figure of merit of detectors is the Noise Equivalent Power (NEP), defined as the minimum input power that can be detected over the level of noise of the device per square root of bandwidth, thus providing a measure of the detector sensitivity. Within drain injection conditions, it can be estimated by using the Nyquist theorem (neglecting any excess noise) as $NEP_d = \frac{\sqrt{4k_BT/R}}{\beta_d}$, being R the device resistance. It is shown in Fig. 2(b) calculated at 1 GHz.

The typical maximum β_d is revealed very close to threshold voltage, as can be observed from the transfer I_D-V_{GS} curve (for a low value of V_{DS}=0.1 V) shown in the right axis [17], [18], [19], while the optimum NEP_d appears for V_{GS} slightly below the maximum β_d, since the increase of R reduces the current noise. It is interesting to note that although the shape and dependence on V_{GS} of the measurements (empty symbols)

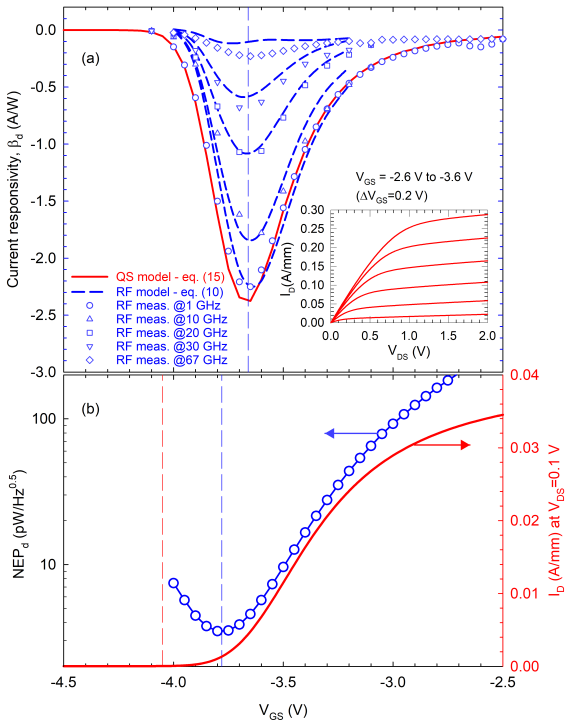

Fig. 2. (a) Current responsivity β_d in A/W measured at different values of the injected frequency (empty symbols) as a function of $\overline{v_{gs}}$ in a AlGaN/GaN HEMT with gate length L_g=250 nm and gate width W=2 × 50 μm. The dashed lines correspond to the results obtained at those frequencies with the proposed model, eq. (10), while the red line corresponds to that of the QS model, eq. (15). The output curves of the transistor are plotted in the inset. (b) NEP_d (blue circles) estimated at 1 GHz and drain current $\overline{i_d}$ measured at $\overline{v_{ds}}$=0.1 V (solid red line, right axis) as a function of $\overline{v_{gs}}$. The dashed vertical reference lines indicate the position of the minimum values of β_d and NEP_d at 1 GHz (blue) and the threshold voltage of the HEMT at $\overline{v_{ds}}$=0.1 V (red).

at higher frequency are very similar to those at 1 GHz, their values decrease progressively, at 67 GHz being one order of magnitude smaller. One of the objectives of this paper is to quantitatively explain this frequency response in terms of the measured S-parameters instead of using a fitting parasitic capacitance [14] or a normalization procedure [9]. Indeed, many papers in the literature of "plasma-wave detectors" compare the RF measurements with theoretical predictions, but it is typically just a qualitative comparison of the V_{GS} dependence, because the input power is not precisely known. This happens mainly in free-space experiments, where the THz (or sub-THz) input signal is coupled to the gate terminal via an antenna. In this work, the RF power is fed either into the gate or the drain ports, with a value which can be exactly calculated thanks to the knowledge of the S-parameters.

B. Proposed RF Model

In the following, time domain variables are lowercase, DC are overlined and complex phasors are uppercase. In order to model the QS detection mechanism of a transistor, the AC component of the drain current is expressed as a two-variable Taylor power series [20], [21], [22] (as a function of v_{gs} and

v_{ds}) of the current-voltage characteristic around the DC bias point $\overline{i_d}$, fixed by $\overline{v_{gs}}$, $\overline{v_{ds}}$, so that:

$$i_d(t) \approx \overline{i_d} + \overline{\Delta i_d} + i_d^{RF}(t) + i_d^{SHG}(t) + \cdots . \quad (1)$$

If the first and second derivatives of the drain current are defined as follows

$$g_{ij} = \frac{\partial^{(i+j)}\overline{i_d}}{\partial^i \overline{v_{gs}} \partial^j \overline{v_{ds}}}, \quad (2)$$

g_{10} being the transconductance, g_m, and g_{01} the drain conductance g_d=1/R, the DC detected current $\overline{\Delta i_d}$ to be recorded by the ampere-meter can be calculated as

$$\overline{\Delta i_d} = \frac{1}{2}\left(\frac{1}{2}g_{20}|V_{gs}|^2 + \frac{1}{2}g_{02}|V_{ds}|^2 + g_{11}\Re\left[V_{gs}V_{ds}^*\right]\right). \quad (3)$$

If an excitation with angular frequency ω=2πf is applied, the linear component $i_d^{RF}(t)$ will depend on the amplitude and phase of the gate and drain voltages V_{gs}=$|V_{gs}|e^{j\varphi_g}$ and V_{ds}=$|V_{ds}|e^{j\varphi_d}$ as

$$i_d^{RF}(t) = g_{10}\Re(V_{gs}) + g_{01}\Re(V_{ds}). \quad (4)$$

The second order component containing second harmonic generation $i_d^{SHG}(t)$ is not developed here.

The key point and one of the main novelties of the model presented in this paper is the precise determination of the voltages at each terminal of the transistor, it is to say, the proper calculation of

$$\begin{aligned} v_{gs}(t) &= \overline{v_{gs}} + \Re(V_{gs}), \\ v_{ds}(t) &= \overline{v_{ds}} + \Re(V_{ds}). \end{aligned} \quad (5)$$

The observable complex voltage V_{xs} at each port (x = gate or drain) is the sum of the progressive and regressive voltage waves V_{xs}^+ and V_{xs}^-. Furthermore, V_{xs}^- can be calculated from V_{xs}^+ thanks to knowledge of the scattering matrix S

$$\begin{pmatrix} V_{gs} \\ V_{ds} \end{pmatrix} = \underbrace{\begin{pmatrix} V_{gs}^+ \\ V_{ds}^+ \end{pmatrix}}_{\text{progressive waves}} + \underbrace{\begin{pmatrix} S_{11} & S_{12} \\ S_{21} & S_{22} \end{pmatrix}\begin{pmatrix} V_{gs}^+ \\ V_{ds}^+ \end{pmatrix}}_{\text{regressive waves}}. \quad (6)$$

If we first focus on the case of drain injection, we must consider that (i) V_{gs}^+=0, since no power is injected into the gate and (ii) V_{ds}^+=$\sqrt{2R_0P_d}$ with R_0=50 Ω the typical output impedance of the source and P_d the available input power. Under these conditions, V_{gs} and V_{ds} can be computed from (6) as

$$V_{ds} = (1 + S_{22})V_{ds}^+; \quad V_{gs} = S_{12}V_{ds}^+. \quad (7)$$

It is important to note that V_{ds} is larger than the injected voltage, as it is the sum of the progressive and the regressive waves. Also, even if no power is injected to the gate (V_{gs}^+=0), the observable gate voltage V_{gs} is not null due to the internal coupling between the gate and the drain, which, in an equivalent circuit representation of the device, would correspond to a C_{gd} capacitance. In order to highlight this phenomena, one can compute the magnitude and phase of the ratio between drain and gate voltages, α_d and θ_d, respectively, as:

$$\alpha_d e^{j\theta_d} = \frac{V_{gs}}{V_{ds}} = \frac{S_{12}}{1 + S_{22}}. \quad (8)$$

Substituting expressions (7) and (8) in (3), the rectified current can be finally expressed as

$$\overline{\Delta i_d} = \frac{1}{2}\left(\frac{1}{2}g_{20}\alpha_d^2 + \frac{1}{2}g_{02} + g_{11}\alpha_d cos(\theta_d)\right)\left|V_{ds}^+\right|^2\left|1 + S_{22}\right|^2, \quad (9)$$

which is almost the same as the one obtained by Khan *et al.* in ref. [21], with one important difference: the presence here of the frequency dependent $|1 + S_{22}|^2$ factor, resulting from the consideration of both injected and reflected waves. Note that the information of the non linearity (considered to be frequency independent) is contained in the coefficients defined in (2), while all the frequency dependence of the RF detector comes from S_{22} and the coupling parameters α_d and θ_d. Using the definition of $V_{ds}^+ = \sqrt{2R_0P_d}$, the responsivity in A/W is

$$\beta_d = \frac{\overline{\Delta i_d}}{P_d} = \frac{R_0}{2}\left(g_{20}\alpha_d^2 + g_{02} + 2g_{11}\alpha_d cos(\theta_d)\right)\left|1 + S_{22}\right|^2, \quad (10)$$

or, using the values of α_d and θ_d calculated from the S-matrix as indicated in (8):

$$\beta_d = \frac{R_0}{2}\left(g_{20}\left|S_{12}\right|^2 + g_{02}\left|1 + S_{22}\right|^2 + 2g_{11}\Re[S_{12}^*(1 + S_{22})]\right). \quad (11)$$

In a similar way, if the power is injected in the gate terminal, so that $V_{ds}^+ = 0$ and $V_{gs}^+ = \sqrt{2R_0P_g}$, we can define

$$\alpha_g e^{j\theta_g} = \frac{V_{ds}}{V_{gs}} = \frac{S_{21}}{1 + S_{11}} \quad (12)$$

and compute the expressions for the responsivity in the case of gate injection as

$$\beta_g = \frac{\overline{\Delta i_d}}{P_g} = \frac{R_0}{2}\left(g_{20} + g_{02}\alpha_g^2 + 2g_{11}\alpha_g cos(\theta_g)\right)\left|1 + S_{11}\right|^2, \quad (13)$$

$$\beta_g = \frac{R_0}{2}\left(g_{20}\left|1 + S_{11}\right|^2 + g_{02}\left|S_{21}\right|^2 + 2g_{11}\Re[S_{21}^*(1 + S_{11})]\right). \quad (14)$$

These are general expressions for the RF detection within both the drain and gate injection schemes, which can be used in any bias condition and in any kind of field effect transistor.

At low frequency, (i) the drain-gate coupling can be neglected ($S_{12} \overset{\omega\to 0}{\approx} 0$ or, equivalently, $\alpha_d \overset{\omega\to 0}{\approx} 0$), and (ii) the drain input reflection coefficient S_{22} tends to the quasi-static reflection coefficient Γ_d, which can be obtained from the drain conductance g_{01}: $S_{22} \overset{\omega\to 0}{\approx} \Gamma_d = \frac{g_{01}^{-1} - R_0}{g_{01}^{-1} + R_0}$. Under these conditions (10) becomes the well known equation for the QS drain responsivity $\beta_d(\omega \to 0)$ plotted in Fig. 2 and published in [17], [18], [19]

$$\beta_d \overset{\omega\to 0}{\approx} \frac{R_0}{2}g_{02}(1 + \Gamma_d)^2 = \frac{1}{2}\frac{g_{02}}{g_{01}}\left(1 - \Gamma_d^2\right). \quad (15)$$

Fig. 2 shows a very good agreement between the RF measurements at 1 GHz in drain-injection conditions (empty blue circles) and the values obtained from eq. (15) (red line). However, as this QS model does not contain any frequency dependence, it is not able to reproduce the RF measurements at high frequencies. The low frequency range where the QS model is valid depends on the device geometry and bias conditions.

IV. Experimental Validation and Physical Interpretation

For validation, the proposed RF model has been implemented in MATLAB software. The g_{ij} coefficients have been calculated by fitting the DC curves of the inset of Fig. 2 to a 5th degree polynomial. For the case of the typical unbiased-drain passive configuration [21] (zero-bias detectors), (i) the value of g_{20} is null (since $\overline{i_d}\approx 0$), and (ii) S_{12}=S_{21}, meaning that gate-drain coupling takes place in both directions (affecting the RF detection in both gate and drain injection conditions) and at the same level.

A. Drain Injection

In the case the RF signal is applied to the drain terminal, eq. (10), or (11), since both are the same, has been used to calculate $\beta_d(f)$ from the measured S-parameters matrix. Fig. 2(a) shows the excellent agreement between the model and the experiments at some selected frequencies in the whole gate-to-source bias range. Moreover, the frequency dependence of β_d shown in Fig. 3(a) at $\overline{v_{gs}}$=−3.65 V (where the peak of β_d is found, see Fig. 2) and $\overline{v_{ds}}$=0 V (zero biased detector condition), confirms again that our model is able to accurately predict the results of the drain-injection RF detection experiments in all the frequency span of the VNA.

Additionally, each of the three contributions of (10) are plotted in Fig. 3(a) in order to understand their respective weight and how significant is the coupling between terminals for the case of drain injection. First, we can see that the dominant term is associated, as expected, to g_{02}. At $\omega\approx 0$, the structural gate-drain capacitance C_{gd} presents very high impedance, leading to a negligible coupling between gate and drain ($\alpha_d\approx 0$), so canceling the contribution of the term associated to g_{11}. Moreover, as explained before, g_{20} is null since $\overline{i_d}\approx 0$ so that the corresponding term in (10) is negligible for all frequencies. As a consequence, the low-frequency plateau observed under drain-injection conditions is provided by the g_{02} term alone (the one considered within the QS model presented in our previous papers) [17], [18], [19].

As the frequency increases, the decrease $vs.$ f of the $|1+S_{22}|^2$ factor, due to the higher drain impedance, leads to a smaller contribution of the term proportional to g_{02}. In parallel, a fraction of the signal injected at the drain reaches the gate thanks to the increasing values of α_d and the term proportional to g_{11} starts to have a significant influence on the final response. Note that both terms have opposite sign, so that the responsivity decreases fast with frequency, with a cutoff frequency of around 19 GHz, due to the addition of both effects. Indeed, at 67 GHz the terms associated to g_{11} (accounting for the drain-gate coupling) and g_{02} (accounting for the direct drain detection), practically cancel each other. In order to remove the effect of the term in g_{11}, a practical solution is to add an external capacitance between gate and source in order to AC ground the gate terminal (so that S_{12}=0 and α_d=0) and thus enhance the responsivity in drain injection configuration [6], [12], [14].

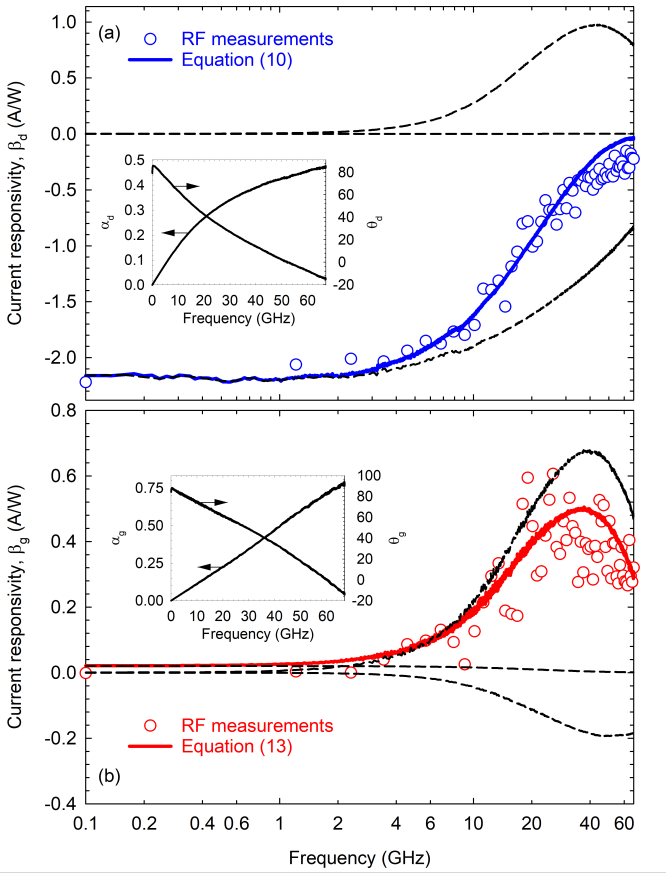

Fig. 3. Drain current responsivity when the RF power is injected at the (a) drain terminal, β_d, given by eq. (10) (blue line) and (b) gate terminal, β_g, given by eq. (13) (red line) as a function of the excitation frequency for $\overline{v_{gs}}$=−3.65 V and $\overline{v_{ds}}$=0 V. RF measurements (star markers) and the three components of the model (dashed lines). The inset represents the coupling parameters: the ratio α (left axis) and the phase shift θ (right axis) between gate and drain voltages.

B. Gate Injection

In the case the RF signal is applied to the gate terminal, eq. (13) (or (14) since both are the same) is used for the calculation of $\beta_g(f)$. The results for $\overline{v_{gs}}$=−3.65 V and $\overline{v_{ds}}$=0 V (the same conditions as for the drain injection case) are shown in Fig. 3(b), where a very good agreement between the measured values and those predicted by our model is observed. At low frequency, the capacitive gate-drain coupling leads to $\alpha_g \overset{\omega\to 0}{\approx} 0$, thereby making, as expected from (13), $\beta_g \overset{\omega\to 0}{\approx} 0$. This happens because a drain voltage is necessary to have an output current, which only builds up at high frequency due to the gate-drain coupling, allowing that part of the input power, as S_{21} increases, reaches the drain. That is why, in order to enhance the detection of low-frequency signals in the gate-injection configuration, practical detectors typically add an external capacitive shunt between the gate and the drain (increasing the effective C_{gd}), so that S_{21} is not null at sufficiently low frequency [8], [23], [13].

The typical assumption in the limit of $1/j\omega C_{gd}\approx 0$ implies that the whole power injected to the gate is propagating to the drain: $\alpha_g\approx 1$ and $\theta_g\approx 0$, as done in ref. [12]. As a consequence

(13) simplifies to

$$\beta_g \approx \frac{R_0}{2}(g_{02}+2g_{11})|1+S_{11}|^2. \quad (16)$$

However, losses and phase shift are inherent to the gate-drain coupling mechanism, so that the previous assumption is too strong for practical cases. Indeed, as shown in the inset of Fig. 3(b), the gate-drain coupling passes from being purely capacitive at $\omega \approx 0$ (α_g=0 and θ_g=90), to practically resistive for the highest frequencies, but with about a 25% voltage drop ($\alpha_g \approx 0.75$ and $\theta_g \approx 0$). This is the typical high-pass filter behaviour of the C_{gd} connecting gate and drain, but with a non-null resistance (and also some inductive parasitics) in series. As can be observed in Fig. 3(b), β_g does not show a plateau at high frequency as predicted by the simplified model of ref. [12]. This is due to the frequency variation of S_{11}, which originates a frequency roll-off before the ideal condition $1/j\omega C_{gd} \approx 0$ is fulfilled. One of the important advantages of the closed-form expressions of the responsivity we are proposing is that (11) and (14) directly taking the S-parameters as a basis, are able not only to provide the complete frequency dependence of the experimental responsivities, but also avoid the need of making strong assumptions such as perfect input matching or absence of parasitics and losses.

At high frequency, the terms in both g_{02} and g_{11} have a significant contribution to the responsivity, and since $g_{02} \approx -g_{11}$, the term in g_{11} becomes the dominant one (note the factor 2 in the calculation). Thus $\beta_g > 0$ due to g_{11}, while $\beta_d < 0$ due to g_{02}. Other authors [23], [24], when using the plasma-wave Dyakonov-Shur theory to explain the results of RF detection in gate injection regime, use a frequency-independent value of β_g proportional to a quantity similar to g_{11}, which is $\frac{d\sigma}{dV_{gs}}$, being σ the conductivity of the channel. By so doing, both the frequency dependent attenuation and the drain contribution to the RF detection are disregarded, but being the input power unknown, a good agreement with the dependence of the measurements on $\overline{v_{gs}}$ (which follows that of g_{11}) is typically obtained by making a normalization.

In order to further confirm the validity of the proposed model, in Fig. 4 we present the results obtained for both β_d and β_g (for the $\overline{v_{gs}}$ providing their maximum values) using HEMTs with different gate geometries (L_g=75, 150 and 250 nm and gate width W=2×25 μm) compared with the results previously presented for the reference HEMTs with L_g=250 nm and gate width W=2×50 μm. For all of them, the agreement between the experiments and the results obtained with equations (10) and (13) is remarkably good. Furthermore, only a weak dependence on the gate length is retrieved, a slightly larger bandwidth is obtained by reducing the gate, with similar responsivity. On the other hand, a significant increase of the responsivity with W is obtained, as β_d and β_g (as g_{20} and g_{11}) are proportional to it, but with a smaller bandwidth [17].

V. Conclusion

In summary, the proposed model provides an excellent agreement with the on-wafer measurements of the current responsivity under both drain and gate injection regimes up to 67 GHz. Moreover, the model may be extended up to frequencies in the terahertz range, as long as the non-linear response measured in DC is at the origin of the detection and other non linear physical phenomena, such as plasma resonance, are not significant. It is also important to remark that the qualitative behaviour shown in Fig. 3 for β_d and β_g for a 250 nm/2×50 μm gate length/width AlGaN/GaN HEMT has been also observed in devices with different gate lengths and widths, and also in InGaAs HEMTs [17].

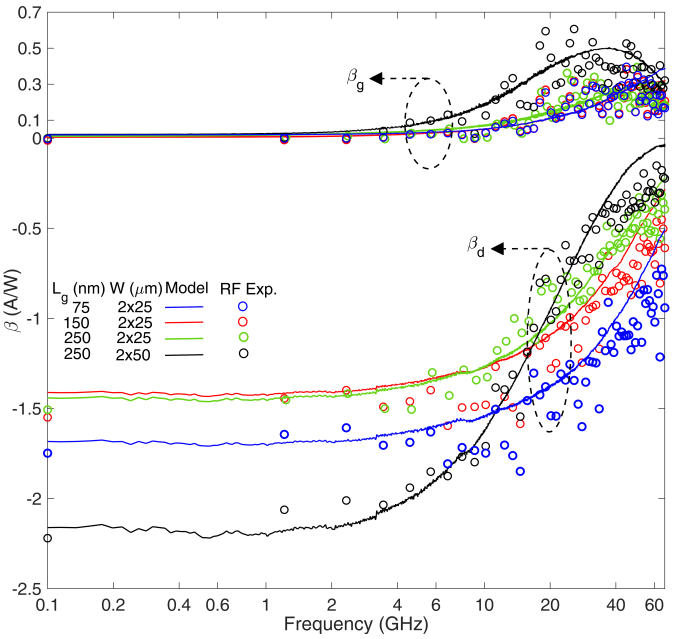

Fig. 4. Measurements of β_d and β_g (circles) compared to the results of the proposed model (lines) given by equations (10) and (13), respectively, as a function of the excitation frequency for HEMTs with different gate geometries: the previously studied one L_g=250 nm and gate width W=2×50 μm, and other three devices with W=2×25 μm and L_g=75, 150 and 250 nm. For each device, the results are presented for the $\overline{v_{gs}}$ value providing a maximum β_d.

Acknowledgment

The authors would like to thank Ó. García-Pérez from the Yebes Observatory at the National Geographic Institute, Guadalajara, Spain, for fruitful discussions about the experimental setup.

References

[1] F. Aniel, G. Auton, D. Cumming, M. Feiginov, S. Gebert, T. González, C. Li, A. Lisauskas, H. Marinchio, J. Mateos, C. Palermo, A. Song, J. Treuttel, L. Varani, and N. Zerounian, *Terahertz Electronic Devices*. Cham: Springer International Publishing, 2023, pp. 807–849. [Online]. Available: https://doi.org/10.1007/978-3-030-79827-7_22

[2] A. Shchepetov, C. Gardès, Y. Roelens, A. Cappy, S. Bollaert, S. Boubanga-Tombet, F. Teppe, D. Coquillat, S. Nadar, N. Dyakonova *et al.*, "Oblique modes effect on terahertz plasma wave resonant detection in InGaAs/InAlAs multichannel transistors," *Appl. Phys. Lett.*, vol. 92, no. 24, Jun. 2008.

[3] S. Blin, L. Tohme, D. Coquillat, S. Horiguchi, Y. Minamikata, S. Hisatake, P. Nouvel, T. Cohen, A. Pénarier, F. Cano *et al.*, "Wireless communication at 310 ghz using GaAs high-electron-mobility transistors for detection," *J. Commun. Netw.*, vol. 15, no. 6, pp. 559–568, Dec. 2013.

[4] S. Kim, D.-W. Park, K.-Y. Choi, and S.-G. Lee, "MOSFET characteristics for terahertz detector application from on-wafer measurement," *IEEE Trans. Terahertz Sci. Technol.*, vol. 5, no. 6, pp. 1068–1077, Nov. 2015.

[5] A. El Fatimy, S. Boubanga Tombet, F. Teppe, W. Knap, D. Veksler, S. Rumyantsev, M. Shur, N. Pala, R. Gaska, Q. Fareed, X. Hu, D. Seliuta, G. Valusis, C. Gaquiere, D. Theron, and A. Cappy, "Terahertz detection by GaN/AlGaN transistors," *Electron. Lett.*, vol. 42, no. 23, p. 1342, Nov. 2006.

[6] M. Bauer, A. Ramer, S. A. Chevtchenko, K. Y. Osipov, D. Cibiraite, S. Pralgauskaite, K. Ikamas, A. Lisauskas, W. Heinrich, V. Krozer, and H. G. Roskos, "A high-sensitivity AlGaN/GaN HEMT terahertz detector with integrated broadband bow-tie antenna," *IEEE Trans. Terahertz Sci. Technol.*, vol. 9, no. 4, pp. 430–444, Jul. 2019.

[7] W. Stillman, C. Donais, S. Rumyantsev, M. Shur, D. Veksler, C. Hobbs, C. Smith, G. Bersuker, W. Taylor, and R. Jammy, "Silicon FinFETs as detectors of terahertz and sub-terahertz radiation," *Int. J. High Speed Electron. Syst.*, vol. 20, no. 01, pp. 27–42, 2011.

[8] A. Zak, M. A. Andersson, M. Bauer, J. Matukas, A. Lisauskas, H. G. Roskos, and J. Stake, "Antenna-integrated 0.6 THz FET direct detectors based on cvd graphene," *Nano Lett.*, vol. 14, no. 10, pp. 5834–5838, Sept. 2014.

[9] J. A. Delgado-Notario, V. Clericò, E. Diez, J. E. Velázquez-Pérez, T. Taniguchi, K. Watanabe, T. Otsuji, and Y. M. Meziani, "Asymmetric dual-grating gates graphene FET for detection of terahertz radiations," *APL Photonics*, vol. 5, no. 6, p. 066102, June 2020.

[10] L. Romeo, D. Coquillat, M. Pea, D. Ercolani, F. Beltram, L. Sorba, W. Knap, A. Tredicucci, and M. S. Vitiello, "Nanowire-based field effect transistors for terahertz detection and imaging systems," *Nanotechnol.*, vol. 24, no. 21, p. 214005, Apr. 2013.

[11] M. Dyakonov and M. Shur, "Detection, mixing, and frequency multiplication of terahertz radiation by two-dimensional electronic fluid," *IEEE Trans. Electron Devices*, vol. 43, no. 3, pp. 380–387, March 1996.

[12] M. A. Andersson and J. Stake, "An accurate empirical model based on volterra series for FET power detectors," *IEEE Trans. Microw. Theory Techn.*, vol. 64, no. 5, pp. 1431–1441, May 2016.

[13] A. Lisauskas, U. Pfeiffer, E. Öjefors, P. H. Bolìvar, D. Glaab, and H. G. Roskos, "Rational design of high-responsivity detectors of terahertz radiation based on distributed self-mixing in silicon field-effect transistors," *J. Appl. Phys.*, vol. 105, no. 11, p. 114511, June 2009.

[14] S. Boppel, A. Lisauskas, M. Mundt, D. Seliuta, L. Minkevicius, I. Kasalynas, G. Valusis, M. Mittendorff, S. Winnerl, V. Krozer, and H. G. Roskos, "CMOS integrated antenna-coupled field-effect transistors for the detection of radiation from 0.2 to 4.3 THz," *IEEE Trans. Microw. Theory Techn.*, vol. 60, no. 12, pp. 3834–3843, Dec. 2012.

[15] J. Federici and L. Moeller, "Review of terahertz and subterahertz wireless communications," *J. Appl. Phys.*, vol. 107, no. 11, p. 111101, 2010. [Online]. Available: https://doi.org/10.1063/1.3386413

[16] J. Marczewski, D. Tomaszewski, M. Zaborowski, and P. Bajurko, "Thermoemission-based model of THz detection and its validation—JLFET case studies," *IEEE Trans. Terahertz Sci. Technol.*, vol. 12, no. 6, pp. 633–647, Nov. 2022.

[17] G. Paz-Martínez, I. Íñiguez-de-la Torre, H. Sánchez-Martín, B. García-Vasallo, N. Wichmann, T. González, and J. Mateos, "Comparison of GaN and InGaAs high electron mobility transistors as zero-bias microwave detectors," *J. Appl. Phys.*, vol. 132, no. 13, p. 134501, Sept. 2022.

[18] G. Paz-Martínez, I. Íñiguez-de-la Torre, H. Sánchez-Martín, J. A. Novoa-López, V. Hoel, Y. Cordier, J. Mateos, and T. González, "Temperature and gate-length dependence of subthreshold RF detection in GaN HEMTs," *Sensors*, vol. 22, no. 4, p. 1515, 2022.

[19] G. Paz-Martínez, I. Íñiguez-de-la Torre, H. Sánchez-Martín, T. González, and J. Mateos, "Analysis of GaN-based HEMTs operating as RF detectors over a wide temperature range," *IEEE Trans. Microw. Theory Techn.*, 2023.

[20] A. Cowley and H. Sorensen, "Quantitative comparison of solid-state microwave detectors," *IEEE Trans. Microw. Theory Techn.*, vol. 14, no. 12, pp. 588–602, Dec. 1966.

[21] M. I. W. Khan, S. Kim, D.-W. Park, H.-J. Kim, S.-K. Han, and S.-G. Lee, "Nonlinear analysis of nonresonant THz response of MOSFET and implementation of a high-responsivity cross-coupled THz detector," *IEEE Trans. Terahertz Sci. Technol.*, vol. 8, no. 1, pp. 108–120, Jan. 2018.

[22] G. J. V.-R. J. e. a. Zhang, X., "Two-dimensional MoS2-enabled flexible rectenna for Wi-Fi-band wireless energy harvesting," *Nature*, vol. 566, no. 7744, p. 368–372, Jan. 2019.

[23] A. Rehman, J. A. Delgado-Notario, P. Sai, D. B. But, P. Prystawko, Y. Ivonyak, G. Cywinski, W. Knap, and S. Rumyantsev, "Temperature dependence of current response to sub-terahertz radiation of AlGaN/GaN and graphene transistors," *Appl. Phys. Lett.*, vol. 121, no. 21, p. 213503, Nov. 2022.

[24] O. A. Klimenko, W. Knap, B. Iniguez, D. Coquillat, Y. A. Mityagin, F. Teppe, N. Dyakonova, H. Videlier, D. But, F. Lime, J. Marczewski, and K. Kucharski, "Temperature enhancement of terahertz responsivity of plasma field effect transistors," *J. Appl. Phys.*, vol. 112, no. 1, p. 014506, Jul. 2012.